ACS Catalysis

Research Article

pubs.acs.org/acscatalysis

Mechanistic Pathway in the Electrochemical Reduction of CO_2 on RuO_2

Mohammadreza Karamad,[†,‡] Heine A. Hansen,[†,⊥] Jan Rossmeisl,[‡] and Jens K. Nørskov*[,†,§]

[†]Department of Chemical Engineering, Stanford University, Stanford, California 94305, United States

[‡]Center for Atomic-scale Materials Design, Department of Physics, Technical University of Denmark, DK-2800 Kongens Lyngby, Denmark

[⊥]Department of Energy Conversion and Storage, Technical University of Denmark, DK-2800 Kongens, Lyngby, Denmark

[§]SUNCAT Center for Interface Science and Catalysis, SLAC National Accelerator Laboratory, 2575 Sand Hill Road, Menlo Park, California 94025, United States

Supporting Information

ABSTRACT: RuO_2 has been reported to reduce CO_2 electrochemically to methanol at low overpotential. Herein, we have used density functional theory (DFT) to gain insight into the mechanism for CO_2 reduction on RuO_2(110). We have investigated the thermodynamic stability of various surface terminations in the electrochemical environment and found CO covered surfaces to be particularly stable, although their formation might be kinetically limited under mildly reducing conditions. We have identified the lowest free energy pathways for CO_2 reduction to formic acid (HCOOH), methanol (CH_3OH), and methane (CH_4) on partially reduced RuO_2(110) covered with 0.25 and 0.5 ML of CO*. We have found that CO_2 is reduced to formic acid, which is further reduced to methanol and methane. At 0.25 ML of CO*, the reduction of formate (OCHO*) to formic acid is the thermodynamically most difficult step and becomes exergonic at potentials below −0.43 V vs the reversible hydrogen electrode (RHE). On the other hand, at 0.5 ML of CO*, the reduction of formic acid to H_2COOH* is the thermodynamically most difficult step and becomes exergonic at potentials below −0.25 V vs RHE. We have found that CO_2 reduction activity on RuO_2 changes with CO coverage, which suggests that CO coverage can be used as a tool to tune the CO_2 reduction activity. We have shown the mechanism for CO_2 reduction on RuO_2 to be different from that on Cu. On Cu, hydrocarbons are formed at high Faradaic efficiency through reduction of CO* at ∼1 V overpotential, while on RuO_2, methanol and formate are formed through reduction of formic acid at lower overpotentials. Using our understanding of the CO_2 reduction mechanism on RuO_2, we suggest reduction of formic acid on RuO_2, which should lead to methanol and methane production at relatively low overpotentials.

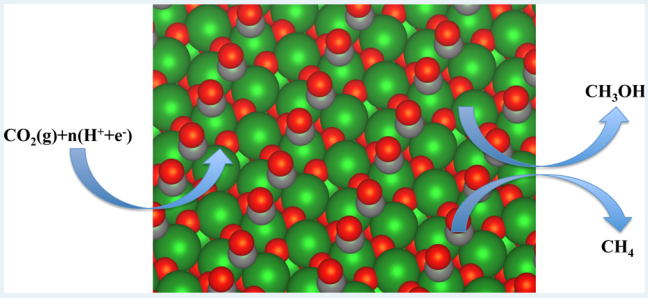

KEYWORDS: *electrocatalysis, CO_2 reduction, methanol synthesis, density functional theory, RuO_2*

INTRODUCTION

Electrochemical reduction of CO_2 (ERCO2) has the potential to enable the storage of power from intermittent renewable energy sources as chemical fuels of high energy density.[1] Three criteria should ideally be met by a catalyst for this reaction to be a cost-effective process: (1) high selectivity toward the desired products, (2) high activity for the formation of the desired products, and (3) high stability under reducing conditions. To date, to the best of our knowledge, no catalyst reported meets these criteria. Therefore, the development of new catalysts is essential, which in turn requires an understanding of the CO_2 reduction mechanism.[2−12]

Several reaction products have been reported for the ERCO2 on pure metals. These products can be classified on the basis of their CO and hydrogen binding energies.[5,13] On metals that bind CO and hydrogen weakly, such as Cd and Hg, formic acid (HCOOH) is the main reaction product. Metals that bind CO and hydrogen strongly, such as Pt and Ni, are selective for evolution of hydrogen. Copper is the only metal with moderate CO and hydrogen binding energies and is the only transition metal that selectively catalyzes the reduction of CO_2 to hydrocarbons, primarily methane (CH_4) and ethylene (C_2H_4), with significant quantities at high current densities.[5] However, ERCO2 on copper requires a high overpotential, making copper an inefficient catalyst for this reaction. ERCO2 to methanol (CH_3OH) is very attractive because methanol is a liquid, which makes it a good candidate for energy storage and automotive applications.[14] However, methanol has not been observed as a major product in CO_2 reduction on pure metals.[5]

Received: October 7, 2014
Revised: May 1, 2015
Published: May 20, 2015

DOI: 10.1021/cs501542n
ACS Catal. 2015, 5, 4075−4081

On the other hand, metal oxide catalysts, such as RuO_2 and Cu_2O, have demonstrated direct ERCO2 to methanol.[15−20] For example, Spataru and co-workers reported ERCO2 on boron doped diamond supported RuO_2 at overpotentials of less than 0.4 V (RHE) and at current densities higher than 1 mA cm^{-2}.[19] However, Cu_2O is not stable under reducing conditions and is reduced alongside CO_2.[15] On the other hand, previous studies have shown that RuO_2 remains stable at reducing potentials.[21,22] Even though RuO_2 has been studied extensively for the oxygen evolution reaction (OER) both experimentally and theoretically,[23,24] there have been, to the best of our knowledge, no theoretical studies on the ERCO2 on RuO_2.

Density functional theory (DFT) calculations in conjunction with the computational hydrogen electrode (CHE) model have been used to elucidate the reaction mechanism as well as intermediates that are involved in the reduction of CO_2 on Cu and late transition metals.[8,9,25,26] Theoretical models have been used to search for catalysts with improved electrocatalytic activity and selectivity.[10,11,27] In the current study, we perform DFT calculations on RuO_2(110) to investigate the mechanism for CO_2 reduction and address why RuO_2 exhibits activity and selectivity toward methanol. To this end, we first identify the thermodynamically stable adsorbate phases of the surface as a function of potential under reaction conditions.[28,29] We find that, at reducing potentials, the RuO_2 surface is partially reduced. Structures covered with CO exhibit high thermodynamic stability, although the formation of CO at high coverage may be kinetically limited. We investigate the reaction mechanism for CO_2 reduction at two different CO coverages on RuO_2(110) and compare the activity and selectivity on RuO_2(110) to those on Cu(211). Our results indicate that HCOOH, CH_4, and CH_3OH are the main reaction products of CO_2 reduction on the RuO_2(110) surface and that CH_4 and CH_3OH are both formed by reduction of adsorbed formic acid (HCOOH*). In contrast, on Cu(211), hydrocarbons are formed through the reduction of CO, while HCOOH is not reduced.

METHODS

Computational Details. The total energies of adsorbates on RuO_2 have been calculated with DFT using the grid-based projector-augmented wave method implemented in the GPAW code and integrated with the atomic simulation environment (ASE).[30,31] Calculations have been performed using the RPBE exchange-correlation functional.[32]

Experimental lattice parameters are a = 4.49 Å and c = 3.10 Å for RuO_2.[33,34] The lattice parameters for RuO_2 in the rutile crystal structure are calculated as a = 4.60 Å and c = 3.10 Å. The slight overestimation (here less than 3%) of lattice parameters is expected, because the RPBE functional tends to overestimate lattice constants.[32] In all calculations, the RuO_2(110) surface was modeled using a four-layer (2 × 1) periodic slab, and the successive slabs were separated by at least 16 Å of vacuum.[24,35] For all calculations, adsorption was only allowed on one side of the slab. One-electron states have been populated at an electronic temperature of k_BT = 0.1 eV and energies extrapolated to T = 0 K for the slab calculations. The first Brillouin zone was sampled using 4 × 4 × 1 Monkhorst−Pack k-points and a grid spacing of 0.18 Å. The bottom two layers were fixed in their bulk structure, while the upper layers and adsorbates were allowed to relax until residual forces in all directions were less than 0.05 eV $Å^{-1}$. Convergence of total energy with respect to grid spacing and the k-point set were considered. The computational hydrogen electrode (CHE) model has been used to calculate the free energy of adsorbates and reaction intermediates.[36] In this model, the free energy change for each reaction step that involves a electron−proton pair transfer at 0 V (RHE) is calculated using the definition that the chemical potential of an electron−proton pair, i.e. $\mu(H^+ + e^-)$, is equal to that of half of the hydrogen in the gas phase at standard pressure: i.e., $1/2[\mu(H_2(g))]$. At potentials different from 0 V (RHE), the chemical potential of the electron is shifted by $-eU$, where e is the elementary charge and U is the electrode potential (RHE). The reaction free energy of an electrochemical step, i, therefore varies linearly with potential U as

$$\Delta G_i(U) = \Delta G_i(U = 0) + eU$$

Additional potential dependence due to variations in dipole moments and polarization of adsorbates may be included as well but have been neglected in the present study, since they tend to be small.[37] According to the CHE model, reaction energies in a reductive pathway are decreased at increasingly negative potentials, and at a certain potential all consecutive steps in the reaction pathway become exergonic. In this scenario, the potential-limiting step is the last step that becomes downhill in free energy. Accordingly, the theoretical working potential is defined as the maximum positive free energy difference between successive electrochemical steps. We note that this model is purely thermodynamic and requires that kinetic barriers for electron−proton transfer be surmountable at room temperature.[38] However, previous theoretical studies of electrochemical reactions have found good correlation between the theoretical overpotential and experimental onset potentials.[24,39,40]

In addition, we want to emphasize that O−H and C−H bond forming reactions could also occur through surface hydrogenation or water-assisted H-shuttling mechanisms, as examined by Nie et al. for CO_2 reduction on Cu(111).[26] They studied barriers for hydrogen transfer to CO_2 reduction intermediates in the presence of water molecules and argued that the dominant pathway to methane and ethylene proceeds through CO reduction to COH. In the case of CO_2 reduction on RuO_2, determining which mechanism in O−H and C−H forming bond reactions dominates requires considering kinetic barriers and is outside the scope of the current study.

We account for solvation corrections by applying the work of Siahrostami et al., which studied the effect of adsorbed water on the oxygen evolution reaction (OER) intermediates, i.e. OH* and OOH*, on different rutile oxides.[41] The corrections accounting for the solvation of OH* and OOH* were reported to be −0.3 and −0.2 eV, respectively. Similarly, to approximate water-induced stabilization in our calculations, we have used a correction of −0.3 eV for OH* and −0.2 eV for adsorbates containing an OH group that indirectly bind to the surface: COOH*, COH*, HCOOH*, and H_2COOH*. Free energies of adsorbates have been calculated assuming the adsorbates are harmonic oscillators. Previous studies have shown that the RPBE functional is poor in describing the reaction energy of gas-phase molecules containing the OCO backbone, whereas the PBE functional gives a poor description of adsorption of the CO molecule.[7,27] It has been shown that the mean absolute errors (MAEs) for CO(g) and gas-phase molecules containing the OCO backbone amount to 0.04 and 0.45 eV, respectively. Therefore, the energy of CO_2(g) has been corrected by 0.45 eV, while no correction has been applied to CO(g).

DOI: 10.1021/cs501542n
ACS Catal. 2015, 5, 4075−4081

RESULTS AND DISCUSSION

Surface Structure under Reaction Conditions. The catalytic activity of the RuO_2 catalyst depends on the atomic structure of the catalyst, which can change with reaction conditions. To gain insight into the surface structures present on RuO_2(110) under reducing conditions, we first consider the thermodynamic stability of surface structures formed in an aqueous electrolyte in the absence of CO_2. The RuO_2(110) surface may be reduced through the exchange of water and protons with the electrolyte through either reduction of surface oxygen

$$O^* + (H^+ + e^-) \rightarrow {}^*OH \quad (1)$$

$${}^*OH + (H^+ + e^-) \rightarrow H_2O + * \quad (2)$$

or adsorption of protons:

$$* + (H^+ + e^-) \rightarrow H^* \quad (3)$$

where * represents a surface site. The RuO_2(110) surface contains two different sites: the coordinatively unsaturated (cus) site, atop the 5-fold coordinated Ru atom, and a site bridging two Ru atoms (see insets in Figure 1) . On the stoichiometric (110) surface, the bridging site is occupied by oxygen, while the cus site is vacant. It is generally found that bridge sites bind adsorbates more strongly than do cus sites.[42] The stability of RuO_2(110) surface terminations formed by exchanges (1)−(3) are shown in Figure 1 relative to the surface, where the bridging oxygen atoms have been reduced to H_2O. The latter surface is also shown as an inset in Figure 1, and we label it "Reduced Surface". It is seen that, below 0 V (RHE), it is favorable to reduce the bridging oxygen atoms present on the stoichiometric surface to H_2O and further cover half of the now empty bridge sites with hydrogen, while the cus sites are vacant (see inset of Figure 1). The latter configuration therefore corresponds to 0.25 ML of H*. At potentials below −0.13 V (RHE), it becomes favorable to cover the bridge sites completely with H*, while still leaving the cus sites vacant, corresponding to a total coverage of 0.5 ML H*. However, it should be noted that, below 0 V (RHE), the production of H_2 by proton reduction becomes thermodynamically favorable and, below the onset potential for the HER, the hydrogen coverage will be determined by the steady-state coverage under HER.

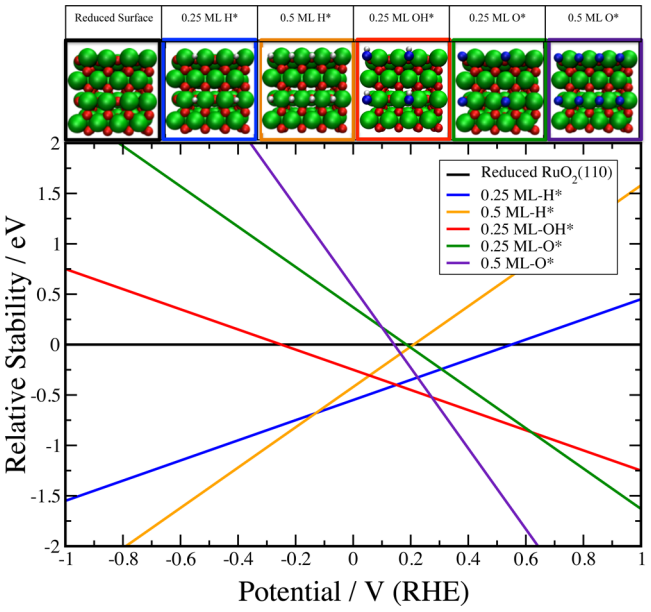

Figure 1. Relative stability of adsorbates formed by proton reduction, i.e. H*, and water oxidation, i.e. O* and OH*, on RuO_2(110) as a function of potential. The insets on the top of the figure show top views of the corresponding surface structures. The solid black line shows the reduced RuO_2(110) surface where all the bridge oxygen atoms have been removed by reduction to H_2O. Ru, bulk oxygen, hydrogen, and carbon atoms are denoted by green, red, white, and gray spheres, respectively. The oxygen atoms of adsorbates are denoted by blue spheres.

Our finding that the RuO_2 surface is partially reduced at 0 and negative potentials is in agreement with XPS experiments.[22] Experimental in situ and *ex situ* XPS studies after the hydrogen evolution on RuO_2 have shown that bulk reduction of RuO_2 to metallic Ru does not occur at potentials above −0.25 V (RHE), as evidenced by the unchanged Ru 3d levels characteristic of the Ru(IV) oxidation state.[21,22] However, the same studies show that the RuO_2 surface may be partially reduced.[22]

In the presence of CO_2, intermediates formed from the reduction of CO_2 may be adsorbed on the bridge and cus sites. Initially, we focus on intermediates formed by one- or two-electron reduction of CO_2. Protonation of CO_2 may happen at an O atom leading to carboxyl

$$* + CO_2 + (H^+ + e^-) \rightarrow COOH^*$$

which may be further reduced to CO

$$COOH^* + (H^+ + e^-) \rightarrow CO^* + H_2O$$

This mechanism for CO production has been suggested to take place on Au and Cu.[7,43] Alternatively, CO_2 may be protonated at the C atom to produce formate

$$* + CO_2 + (H^+ + e^-) \rightarrow OCHO^*$$

which may be further protonated to formic acid[7]

$$OCHO^* + (H^+ + e^-) \rightarrow HCOOH^*$$

whereas protonation to OCH_2O^* is usually thermodynamically difficult.

Figure 2 shows the stability of the above intermediates at various coverages on the partially reduced RuO_2(110) surface. It is seen that CO* acts as a thermodynamic sink, with 0.5 ML of CO* becoming the most stable surface termination below 0.28 V (RHE) and the CO* coverage further increasing to 0.75 ML of CO* below −0.05 V (RHE). The reduction of CO* through formation of either COH* and CHO* is difficult and requires potentials below −0.84 V (RHE) to become thermodynamically favorable on the surface with 0.75 ML of CO*. The removal of CO* through desorption will be slow due to the strong CO binding. The desorption energy is 1.88 and 0.94 eV at 0.25 and 0.75 ML of CO*, respectively. Slow CO desorption is consistent with the very low Faradaic efficiency observed for CO production on RuO_2.[19] The high stability and difficult removal of CO* suggest that CO* will build up on the electrode under CO_2 reduction. However, CO* is formed through the COOH* intermediate, which is rather unstable; thus, the formation of CO* may not always be kinetically accessible. Formation of 0.25 ML of COOH* becomes thermodynamically favorable at potentials below −0.02 V (RHE) on the surface where the bridging oxygen

DOI: 10.1021/cs501542n
ACS Catal. 2015, 5, 4075−4081

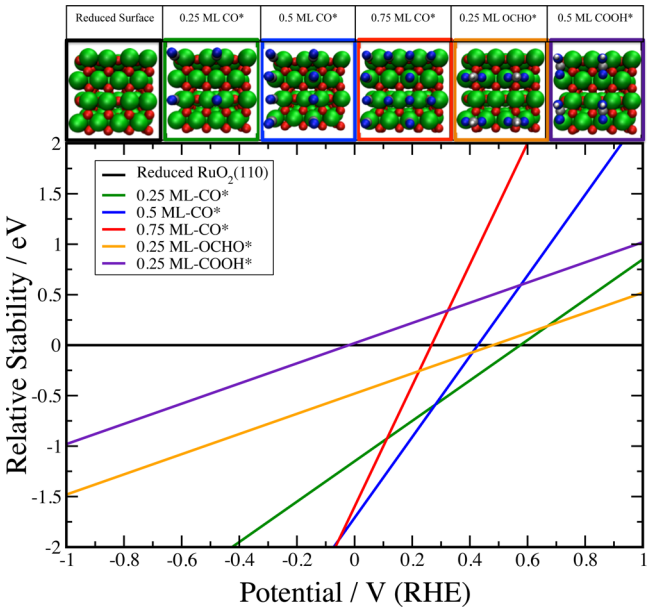

Figure 2. Relative stability of CO_2 reduction intermediates, including CO*, OCHO*, and COOH*, on RuO_2(110) as a function of potential. The insets show top views of the corresponding surface structures. Ru, bulk oxygen, hydrogen, and carbon atoms are denoted by green, red, white, and gray spheres, respectively. The oxygen atoms of adsorbates are denoted by blue spheres.

atoms have been reduced to H_2O, while formation of 0.25 ML of COOH* becomes thermodynamically favorable at potentials below −0.41 V (RHE) on the surface with 0.25 ML of CO* (Figure S2 in Supporting Information).

It is usually found that electrochemical reactions have onsets close to the limiting potential where reaction steps become thermodynamically favorable.[7,36] Consequently, we at least expect the formation of 0.25 ML of CO* to be kinetically accessible below −0.02 V (RHE), while the formation of 0.5 ML of CO* is kinetically accessible below −0.41 V (RHE). However, depending on the time scale of the electrolysis experiment, these CO* coverages likely become accessible at more positive potentials, because it is not necessary to sustain fast steady-state CO* production in order to produce about 0.5 ML of CO* to adsorb strongly on the catalyst surface without desorption. Due to the uncertainties in the CO* coverage under reaction conditions, we investigate in the following the mechanism for CO_2 reduction on the surfaces with 0.25 and 0.5 ML of CO*, which we take as limits of low and high CO coverages, respectively.

Mechanism for CO_2 Reduction on RuO_2(110). In this section, we examine the electrocatalytic activity of CO_2 reduction on the surface structures with 0.25 and 0.5 ML of CO*. We inspect several possible reaction intermediates and construct free energy diagrams corresponding to different reaction pathways.[7] These reaction intermediates along with possible reaction pathways are provided in the Supporting Information. These free energy diagrams provide insight into the mechanism for CO_2 reduction on RuO_2 as well as activity and selectivity. Here we focus on the lowest-energy pathways for the formation of HCOOH, CH_4 and CH_3OH, at low and high CO* coverages. Full information about competing pathways is provided in the Supporting Information. We note that the hydrogen evolution reaction (HER) competes with CO_2 reduction. However, since the focus of the present work is to gain insight into the mechanistic pathway of CO_2 reduction, HER is not considered in the present study.

Low CO Coverage.* Figure 3 shows the lowest-energy pathways for the formation of HCOOH, CH_4, and CH_3OH at 0 potential vs RHE on RuO_2(110) at low CO* coverage. Figure 3a shows the reaction pathway to HCOOH. The protonation of CO_2 results in the formation of formate, OCHO*, or carboxyl, COOH*. While formation of COOH* is endergonic by 0.41 eV, formation of OCHO* is exergonic by 0.46 eV. The second electron−proton transfer results in the formation of formic acid, HCOOH*, on the bridge site. With a desorption energy of 0.3 eV, HCOOH* desorbs easily from the bridge site, and the desorption rate of HCOOH* will be high at ambient temperatures. A second pathway to formic acid is reduction of OCHO* on the cus site. In this route, where OCHO* adsorbed on the bridge site is a spectator, CO_2 reduces to OCHO* on the cus site and then to formic acid. This pathway may be responsible for formic acid formation at more negative potentials: i.e., below −0.53 V where the reduction of CO_2 to OCHO* on the cus site occurs.

After formation of HCOOH*, further electron−proton transfer to HCOOH* might be possible before breaking an oxygen−carbon bond and producing hydrocarbons or alcohols. Figure 3b and 3c show the lowest-energy pathways for the reduction of HCOOH*. The first electron−proton transfer to HCOOH* could take place with protonation of either the C or O atoms; however, we found that the latter has a lower energy pathway than the former. Therefore, the electron−proton transfer to HCOOH* results in the formation of H_2COOH*, which adsorbs with the oxygen binding to the bridge site and the hydroxyl group coordinated to the cus site. In the next protonation step, H_2COOH* is protonated to form adsorbed methoxy (CH_3O*) and hydroxyl (OH*) that bind to the bridge and cus sites, respectively. At this stage, the selectivity toward methanol or methane production is determined. That is, by protonation of carbon atom in the adsorbed methoxy group, methane forms, leaving adsorbed oxygen behind. The hydroxyl and oxygen are reduced to water after one and two electron−proton transfer steps, respectively. On the other hand, methanol forms by protonation of the oxygen atom in the adsorbed methoxy group. The adsorbed hydroxyl is protonated to form water. As shown in Figure 3b and 3c, from a thermodynamic standpoint, formation of both methanol and methane from methoxy pathways are downhill in free energy. This is in agreement with the experimental results, where both methanol and methane were observed as $ERCO_2$ products on RuO_2.[19] However, the Faradaic efficiency for methanol was reported to be higher than that for methane, which is in qualitative agreement with the reduction to methanol being thermodynamically favored over the reduction to methane. Differences in kinetic barriers may, however, also play a role that needs to be explored in future studies. The potential-limiting step in both methanol and methane formation from CO_2 is the protonation of OCHO* to form HCOOH*, and the change in free energy corresponding to this step is 0.43 eV at 0 V (RHE), which results in a limiting potential of −0.43 V (RHE). We note that this potential is similar to the potential needed to reduce COOH* to CO* on the surface with 0.25 ML of CO*. This means that, at this potential, ERCO2 occurs on the surface with 0.5 ML of CO*. However, if the barrier to form COOH* is high, the transient for reaching steady-state coverage of 0.5 ML of CO* may also be long: i.e., the coverage of 0.25 ML of CO* is the relevant coverage during an

DOI: 10.1021/cs501542n
ACS Catal. 2015, 5, 4075−4081

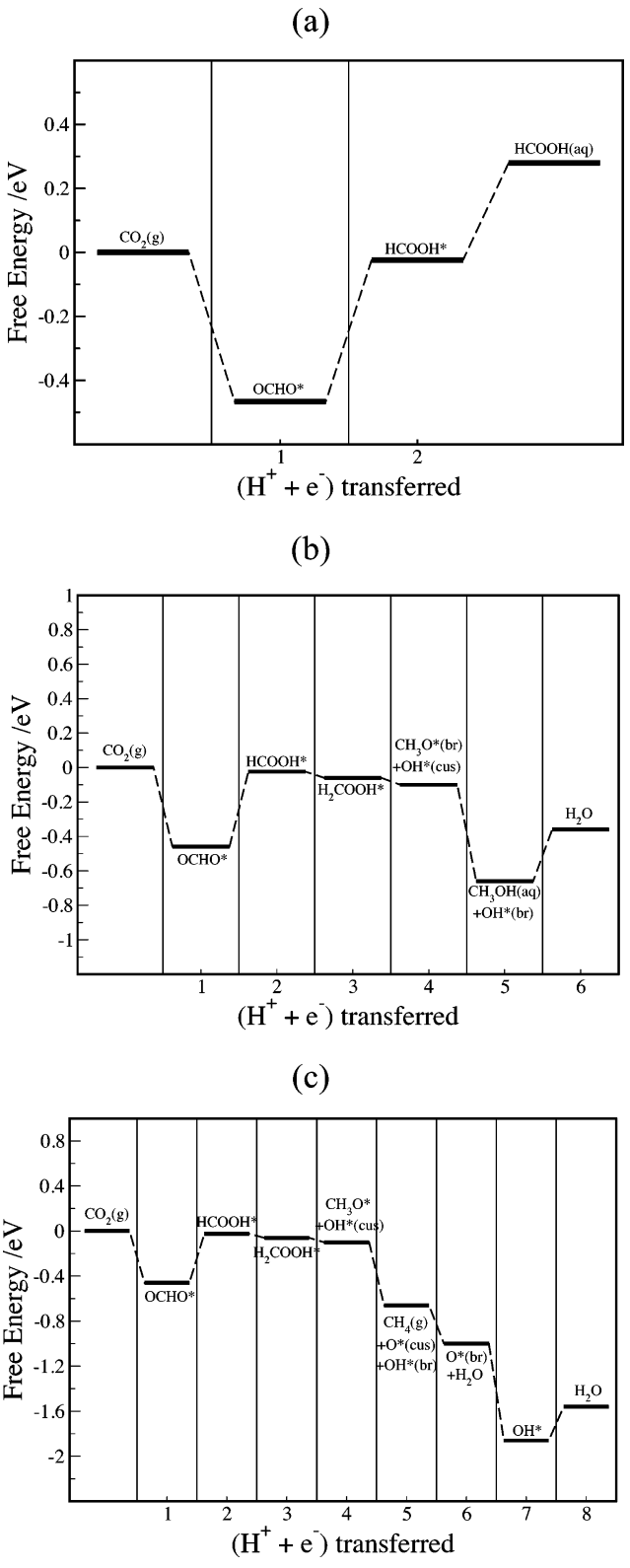

Figure 3. Free energy diagram for the lowest energy pathways to (a) HCOOH(aq), (b) CH_3OH(aq), and (c) CH_4(g) at 0 V (RHE) on RuO_2(110) at low CO* coverage. (br) and (cus) stand for bridge and cus sites, respectively. Concentrations of 8.4 and 1 mM were assumed for HCOOH(aq) and CH_3OH(aq), respectively, following ref 19.

experiment. On the other hand, when the time scale for reaching steady-state 0.5 ML CO* coverage is long, the coverage of 0.5 ML of CO* is the relevant CO* coverage during an experiment.

High CO Coverage.* Figure 4a shows the lowest free-energy pathway to HCOOH on RuO_2(110) at high CO* coverage.

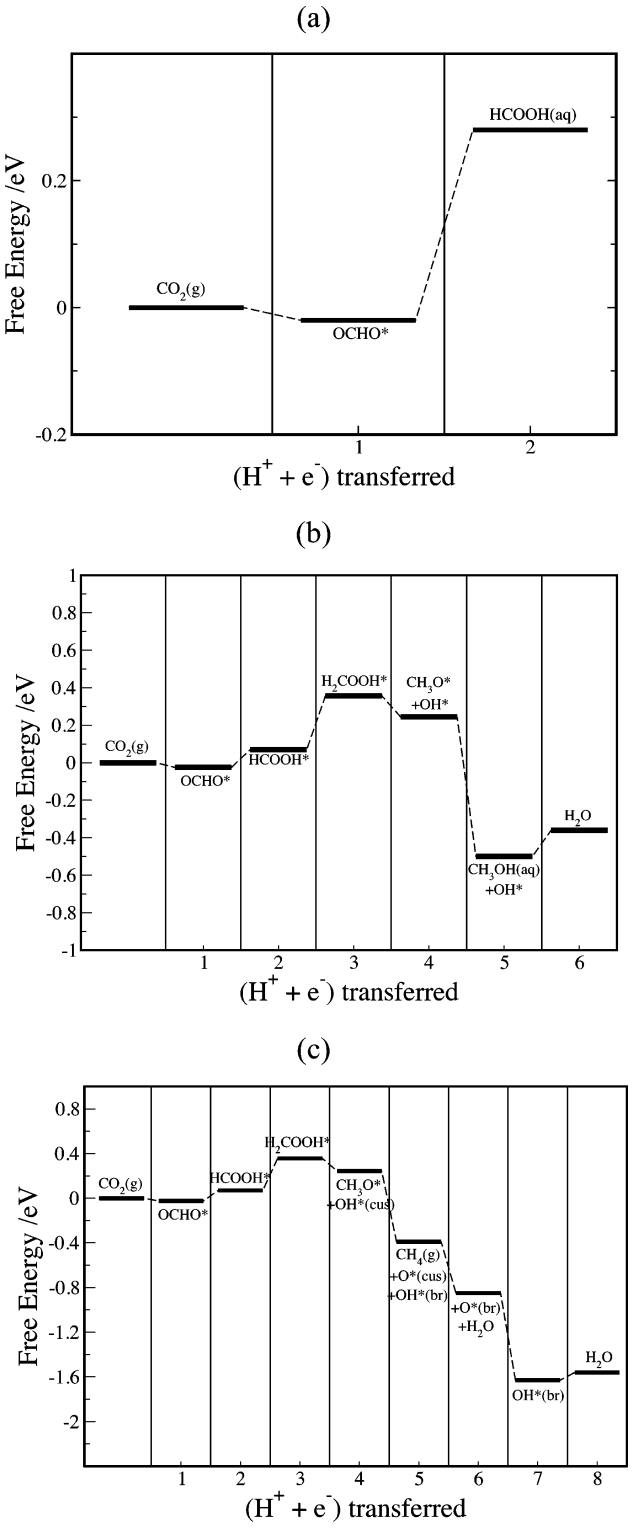

Figure 4. Free energy diagrams for the lowest energy pathways to (a) HCOOH(aq), (b) CH_3OH(aq), and (c) CH_4(g) at 0 V (RHE) on RuO_2(110) at high CO* coverage. (br) and (cus) stand for bridge and cus sites, respectively. Concentrations of 8.4 and 1 mM were assumed for HCOOH(aq) and CH_3OH(aq), respectively, following ref 19.

DOI: 10.1021/cs501542n
ACS Catal. 2015, 5, 4075−4081

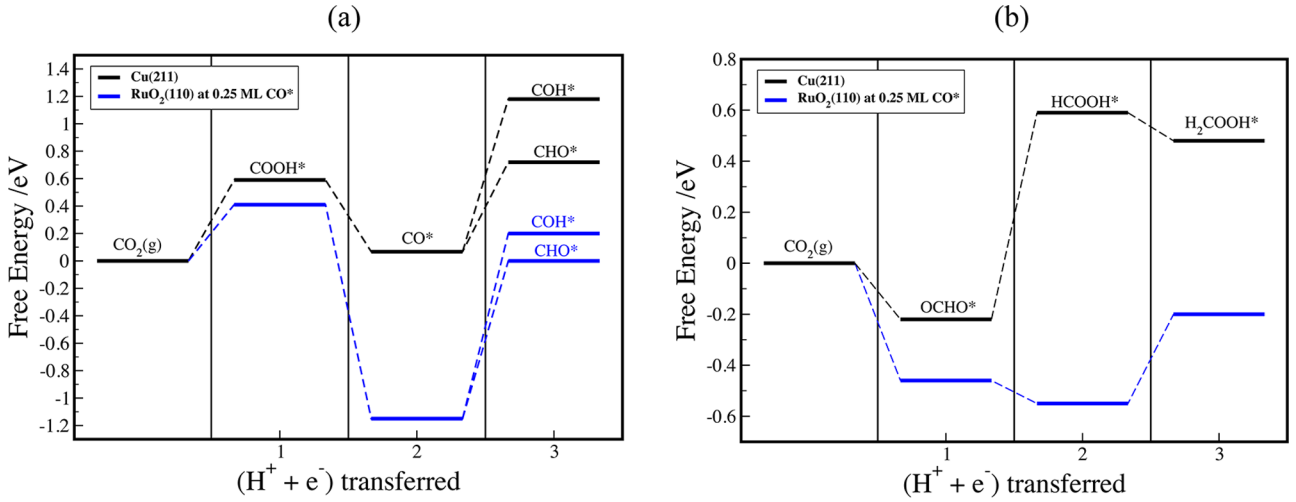

Figure 5. Free energy diagrams on Cu(211) and RuO_2(110) with low CO* coverage at 0 V (RHE) for the first three intermediates in the reduction of CO_2 to (a) CHO*/COH* and (b) H_2COOH*.

Reduction of CO_2 to HCOOH at high CO* coverage follows the same reaction pathway as that at low CO* coverage. The first electron−proton transfer to CO_2 results in the formation of formate, OCHO*, and is slightly exergonic at 0 V (RHE). On the other hand, formation of COOH* is endergonic by 0.7 eV, hindering formation of CO* at significant rates, and hence there is an increase in the coverage of CO* at low overpotentials. The second electron−proton transfer results in the formation of formic acid, HCOOH*, adsorbed on the bridge site. With a desorption energy of 0.3 eV, HCOOH* desorbs easily from the bridge site, and the desorption rate of HCOOH* will be high at ambient temperatures.

Further protonation of HCOOH* proceeds through H_2COOH*, similar to low CO* coverage, and the final reaction products are methanol and methane, as shown in Figure 4b and 4c. However, the potential-limiting step is the protonation of HCOOH* to H_2COOH*. The reaction free energy for this step is 0.28 eV at 0 V (RHE), resulting in a lower negative limiting potential of −0.28 V (RHE) for methanol and methane formation at high CO* coverage. Moreover, as can be seen from Figure 4b and 4c, the formation of both methanol and methane from methoxy pathways are downhill in free energy, and the former is favored over the latter by 0.35 eV. We speculate that the changes in the overpotential and the potential-limiting step at high CO* coverage are due to the increased repulsion from adsorbed CO on the neighboring site when CO* coverage increases from 0.25 to 0.5 ML.

CO_2 Reduction on Cu(211) versus RuO_2(110). In this section we compare the mechanism for CO_2 reduction on RuO_2(110) to that on Cu(211).

As mentioned above, our analysis throughout the present work is solely based on the reaction free energies. From calculations of the hydrogenation barriers in the presence of water, Nie et al.[26] have argued that, on Cu(111), CO_2 reduction proceeds through COH rather than CHO. On the other hand, Durand et al.[9] have shown that, from a thermodynamic standpoint, formation of COH* is less favorable than CHO* on both Cu(111) and Cu(211) surfaces. While exploring the role of reaction kinetics for both protonation and surface hydrogenation is essential in determining if COH* formation is favored over CHO* on Cu(211), from a thermodynamic point of view with our methodology, CHO* is more stable than COH*. Similarly on RuO_2(110), CHO* binds 0.1 eV more strongly than does COH*. However, due to the uncertainty for Cu(211), we have considered both CHO* and COH* as possible intermediates in the $ERCO_2$.

Figure 5 shows the calculated lowest-energy pathways for CO_2 reduction on Cu(211) and RuO_2(110) at low CO* coverage.[7,9] As can be seen in Figure 5, reduction of CO_2 on Cu and RuO_2 proceed through different pathways. On RuO_2, reduction of CO_2 proceeds through HCOOH*; its formation is the potential-limiting step, and CO is not a reaction intermediate in the production of CH_3OH. On the other hand, in the $ERCO_2$ on Cu, HCOOH* is not an intermediate in the production of CH_4. Instead, CO* is a key intermediate; its protonation is the potential-limiting step for formation of CH_4.[7,9,26]

Moreover, our calculations predict higher catalytic activity for CO_2 reduction on RuO_2 in comparison to that on Cu. The theoretical limiting potentials for $ERCO_2$ on RuO_2 are −0.43 and −0.28 V (RHE) for low and high CO* coverage limits, respectively.

CONCLUSION

Experimental studies have shown that CO_2 is reduced to methanol on RuO_2.[17,19] In the current theoretical study, we find that partial reduction of the RuO_2 surface is thermodynamically favorable at negative potentials. Our calculations show that 0.25 ML CO* and 0.5 ML CO* covered RuO_2 surface structures exhibit high thermodynamic stability during CO_2 reduction. However, long-time-scale experiments are needed to reach steady-state CO* coverages. CO poisoning may become an issue under long-term electrolysis at more reducing potentials. By constructing the lowest free energy pathways for the $ERCO_2$ at low and high CO* coverages, we find that $ERCO_2$ reactions at low and high CO* coverages follow identical reaction pathways, though with different potential-limiting steps. The $ERCO_2$ to methanol and methane proceeds through reduction of formic acid, HCOOH*. The calculated theoretical limiting potentials for $ERCO_2$ to methanol and methane are −0.43 and −0.28 V (RHE) at low and high CO* coverages, respectively. At low CO* coverage, the potential-limiting step is protonation of OCHO* to form HCOOH*, while that at high CO*

DOI: 10.1021/cs501542n
ACS Catal. 2015, 5, 4075−4081

coverage is the protonation of HCOOH* to form H_2COOH*. Subsequently, the reduction of formic acid on RuO_2 should lead to methanol and methane production at relatively low overpotentials. Since the formic acid coverage depends on the local concentration of formic acid near the cathode, the formic acid flow rate could affect the overall reaction rate. The pathway for CO_2 reduction on RuO_2 is in stark contrast with that on Cu, where (1) methane and ethylene are the main reduction products of $ERCO_2$, (2) HCOOH* is not an intermediate in the reduction of CO_2 to methane and ethylene, (3) formic acid is not reduced, and (4) CO* is an inevitable intermediate whose protonation is the potential-limiting step. Our proposed pathway is compatible with experimental data for $ERCO_2$ on a RuO_2 electrode. However, other factors such as reaction kinetics and explicit inclusion of the solvation effects need to be further investigated.

■ ASSOCIATED CONTENT

Supporting Information

The Supporting Information is available free of charge on the ACS Publications website at DOI: 10.1021/cs501542n.

Further details of the DFT calculations and reaction pathways (PDF)

■ AUTHOR INFORMATION

Corresponding Author

*E-mail for J.K.N.: norskov@stanford.edu.

Notes

The authors declare no competing financial interest.

■ ACKNOWLEDGMENTS

The authors acknowledge support from the Global Climate Energy Project (GCEP) at Stanford University (Fund No. 52454).

■ REFERENCES

(1) Lewis, N. S.; Nocera, D. G. *Proc. Natl. Acad. Sci. U. S. A.* **2006**, *103*, 15729−15735.
(2) Hori, Y.; Kikuchi, K.; Murata, A.; Suzuki, S. *Chem. Lett.* **1986**, *15*, 897−898.
(3) Hori, Y.; Murata, A.; Takahashi, R.; Suzuki, S. *J. Am. Chem. Soc.* **1987**, *109*, 5022−5023.
(4) Hori, Y.; Murata, A.; Takahashi, R. *J. Chem. Soc., Faraday Trans. 1* **1989**, *85*, 2309−2326.
(5) Hori, Y. CO_2 Reduction on Metal Electrodes. In *Modern Aspects of Electrochemistry*; Vayenas, C. G., White, R. E., Gamboa-Aldeco, M. E., Eds.; Springer: New York, 2008; pp 89−189.
(6) Schouten, K. J. P.; Kwon, Y.; van der Ham, C. J. M.; Qin, Z.; Koper, M. T. M. *Chem. Sci.* **2011**, *2*, 1902−1909.
(7) Peterson, A. A.; Abild-Pedersen, F.; Studt, F.; Rossmeisl, J.; Nørskov, J. K. *Energy Environ. Sci.* **2010**, *3*, 1311−1315.
(8) Peterson, A. A.; Nørskov, J. K. *J. Phys. Chem. Lett.* **2012**, *3*, 251−258.
(9) Durand, W. J.; Peterson, A. A.; Studt, F.; Abild-Pedersen, F.; Nørskov, J. K. *Surf. Sci.* **2011**, *605*, 1354−1359.
(10) Karamad, M.; Tripkovic, V.; Rossmeisl, J. *ACS Catal.* **2014**, *4*, 2268−2273.
(11) Chan, K.; Tsai, C.; Hansen, H. A.; Nørskov, J. K. *ChemCatChem* **2014**, *6*, 1899−1905.
(12) Montoya, J. H.; Peterson, A. A.; Nørskov, J. K. *ChemCatChem* **2013**, *5*, 737−742.
(13) Gattrell, M.; Gupta, N.; Co, A. *J. Electroanal. Chem.* **2006**, *594*, 1−19.
(14) Olah, G. A. *Angew. Chem., Int. Ed.* **2005**, *44*, 2636−2639.
(15) Le, M.; Ren, M.; Zhang, Z.; Sprunger, P. T.; Kurtz, R. L.; Flake, J. C. *J. Electrochem. Soc.* **2011**, *158*, E45.
(16) Frese, K. W. *J. Electrochem Soc.* **1991**, *138*, 3338−3344.
(17) Bandi, A. *J. Electrochem. Soc.* **1990**, *137*, 2157−2160.
(18) Popić, J. P.; Avramov-Ivić, M. L.; Vuković, N. B. *J. Electroanal. Chem.* **1997**, *421*, 105−110.
(19) Spataru, N.; Tokuhiro, K.; Terashima, C.; Rao, T. N.; Fujishima, A. *J. Appl. Electrochem.* **2003**, *33*, 1205−1210.
(20) Qu, J.; Zhang, X.; Wang, Y.; Xie, C. *Electrochim. Acta* **2005**, *50*, 3576−3580.
(21) Rochefort, D.; Dabo, P.; Guay, D.; Sherwood, P. M. A. *Electrochim. Acta* **2003**, *48*, 4245−4252.
(22) Kötz, E. R.; Stucki, S. *J. Appl. Electrochem.* **1987**, *17*, 1190−1197.
(23) Rossmeisl, J.; Qu, Z.-W.; Zhu, H.; Kroes, G.-J.; Nørskov, J. K. *J. Electroanal. Chem.* **2007**, *607*, 83−89.
(24) Man, I. C.; Su, H.-Y.; Calle-Vallejo, F.; Hansen, H. A.; Martínez, J. I.; Inoglu, N. G.; Kitchin, J.; Jaramillo, T. F.; Nørskov, J. K.; Rossmeisl, J. *ChemCatChem* **2011**, *3*, 1159−1165.
(25) Calle-Vallejo, F.; Koper, M. T. M. *Angew. Chem., Int. Ed.* **2013**, *52*, 7282−7285.
(26) Nie, X.; Esopi, M. R.; Janik, M. J.; Asthagiri, A. *Angew. Chem., Int. Ed.* **2013**, *52*, 2459−2462.
(27) Tripkovic, V.; Vanin, M.; Karamad, M.; Björketun, M. E.; Jacobsen, K. W.; Thygesen, K. S.; Rossmeisl, J. *J. Phys. Chem. C* **2013**, *117*, 9187−9195.
(28) Hansen, H. A.; Rossmeisl, J.; Nørskov, J. K. *Phys. Chem. Chem. Phys.* **2008**, *10*, 3722−3730.
(29) Su, H.-Y.; Gorlin, Y.; Man, I. C.; Calle-Vallejo, F.; Nørskov, J. K.; Jaramillo, T. F.; Rossmeisl, J. *Phys. Chem. Chem. Phys.* **2012**, *14*, 14010−14022.
(30) Mortensen, J.; Hansen, L.; Jacobsen, K. *Phys. Rev. B: Condens. Matter Mater. Phys.* **2005**, *71*, 035109.
(31) *Atomic Simulation Environment (ASE)*; Center for Atomic-scale Materials Design (CAMD), Technical University of Denmark, Lyngby, Denmark; https://wiki.fysik.dtu.dk/ase.
(32) Hammer, B.; Hansen, L.; Nørskov, J. *Phys. Rev. B: Condens. Matter Mater. Phys.* **1999**, *59*, 7413−7421.
(33) Atanasoska, L.; O'grady, W. E.; Atanasoski, R. T.; Pollak, F. H. *Surf. Sci.* **1988**, *202*, 142−166.
(34) Hong, S.; Karim, A.; Rahman, T. S.; Jacobi, K.; Ertl, G. *J. Catal.* **2010**, *276*, 371−381.
(35) Rossmeisl, J.; Logadottir, A.; Nørskov, J. K. *Chem. Phys.* **2005**, *319*, 178−184.
(36) Nørskov, J. K.; Rossmeisl, J.; Logadottir, A.; Lindqvist, L.; Kitchin, J. R.; Bligaard, T.; Jónsson, H. *J. Phys. Chem. B* **2004**, *108*, 17886−17892.
(37) Karlberg, G. S.; Rossmeisl, J.; Nørskov, J. K. *Phys. Chem. Chem. Phys.* **2007**, *9*, 5158−5161.
(38) Skúlason, E.; Tripkovic, V.; Björketun, M. E.; Gudmundsdóttir, S.; Karlberg, G.; Rossmeisl, J.; Bligaard, T.; Jónsson, H.; Nørskov, J. K. *J. Phys. Chem. C* **2010**, *114*, 18182−18197.
(39) Nørskov, J. K.; Bligaard, T.; Logadottir, A.; Kitchin, J. R.; Chen, J. G.; Pandelov, S.; Stimming, U. *J. Electrochem. Soc.* **2005**, *152*, J23.
(40) Greeley, J.; Stephens, I. E. L.; Bondarenko, A. S.; Johansson, T. P.; Hansen, H. A.; Jaramillo, T. F.; Rossmeisl, J.; Chorkendorff, I.; Nørskov, J. K. *Nat. Chem.* **2009**, *1*, 552−556.
(41) Siahrostami, S.; Vojvodic, A. *J. Phys. Chem. C* **2014**, *119*, 1032−1037.
(42) Rossmeisl, J.; Logadottir, A.; Nørskov, J. K. *Chem. Phys.* **2005**, *319*, 178−184.
(43) Noda, H. N.; Ikeda, S.; Yamamoto, A.; Einaga, H.; Ito, K. *Bull. Chem. Soc. Jpn.* **1995**, *68*, 1889−1895.

DOI: 10.1021/cs501542n
ACS Catal. 2015, 5, 4075−4081